Transistor-Like Behavior of a Bose-Einstein Condensate in a Triple Well Potential.

James A. Stickney and Alex A. Zozulya
Department of Physics, Worcester Polytechnic Institute, 100 Institute Road, Worcester, Massachusetts 01609

Dana Z. Anderson
Department of Physics and JILA, University of Colorado and National Institute of Standards and Technology, Boulder, Colorado 80309-0440

In the last several years considerable efforts have been devoted to developing Bose-Einstein Condensate (BEC)-based devices for applications such as fundamental research, precision measurements and integrated atom optics. Such devices capable of complex functionality can be designed from simpler building blocks as is done in microelectronics. One of the most important components of microelectronics is a transistor. We demonstrate that Bose-Einstein condensate in a three well potential structure where the tunneling of atoms between two wells is controlled by the population in the third, shows behavior similar to that of an electronic field effect transistor. Namely, it exhibits switching and both absolute and differential gain. The role of quantum fluctuations is analyzed, estimates of switching time and parameters for the potential are presented.

PACS numbers: 32.80.Pj, 03.75.Kk, 85.30.Tv

I. INTRODUCTION

Recent experimental realizations of atom optical devices such as atomic waveguides, beamsplitters [1, 2, 3, 4], on-chip BEC sources and conveyor belts [5, 6] opens a way for development of more complex devices such as, e.g., BEC-based interferometers [7, 8]. On-chip integrated cold atom circuits capable of complex functionality can be constructed from simpler building blocks as it is done in microelectronics to find applications in fundamental physics, precision measurements and quantum information technology.

One of the most important components of a microelectronic circuit is a transistor. In this paper we present a BEC-based device which will be subsequently called a BEC transistor or an atom transistor. It enables one to control a large number of atoms with a smaller number of atoms and demonstrates switching and both differential and absolute gain thus showing behavior similar to that of an electronic transistor. The device is not optimized for performance but is arguably the simplest possible geometry showing behavior reminiscent of a transistor. This makes its experimental realization relatively easy with existing atom chip techniques.

The BEC transistor uses a Bose Einstein condensate in a triple well potential, as shown schematically in Fig 1. In fact, Fig. 1 refers to two subtly different possible experimental realization of the device. In the trapped configuration, the BEC is confined in all three dimensions in the potential wells. The wells are allowed to interact for time interval T. This is done either spatially bringing them together and separating apart after time T of changing the shapes of the potential wells so that the interaction is suppressed after time T. In the waveguide configuration, the potential wells of Fig. 1 represent three guides that converge, run parallel to each other for distance L and then diverge. The interaction time $T = L/v$ in this geometry is determined by the speed of flow v of the BEC in the guides. In the following for definiteness we will use the terminology appropriate for the trapped configuration.

The BEC transistor is similar to an electronic field effect transistor. The left well behaves like the source, the middle as the gate, and the right well is equivalent to the drain. If there are no atoms in the middle well, practically no atoms tunnel from the left into the right well, as shown in Fig. 1a. A small number of atoms placed into the middle well switches the device resulting into the strong flux of atoms from the left well (the source) through the middle and into the right well as shown in Fig. 1b. Increasing number of atoms in the middle well increases the number of atoms that tunnel into the right well. Parameters of the triple well structure are chosen so that the number of atoms having tunneled into the right well at the end of the interaction period is much larger that the number of atoms in the middle well. In the subsequent sections we will show that the BEC transistor exhibits both absolute and differential gain.

The physics of operation of the BEC transistor is based on atom-atom interactions and appropriate design of the potentials. The chemical potential of the left well is chosen to be nearly equal to the ground state energy level of the empty right well (in Fig. 1 we make them equal). The ground state energy of the empty middle well is chosen to be considerably lower than that in both the left and the right wells. Placing atoms in a well raises the value of chemical potential due to atom-atom interactions. Parameters of the potential wells are chosen so that the chemical potential in the middle well is considerably more sensitive to the change in the number of atoms in the well than is the case for the left and right wells.

When the middle and right wells are initially unpopulated, tunneling of atoms from the left to the middle

well is blocked because of the energy mismatch as shown in Fig. 1c. If some amount of atoms is placed into the middle well, the atom-atom interactions will increase the energy of the atoms in the middle well. When the chemical potential in the middle well becomes nearly equal to that in the left and right wells, the device switches and atoms become able to tunnel from the left through the middle into the right well as shown in Fig. 1d.

Using atom-atom interactions to block tunneling in a double-well structure is often referred to as self trapping. This effect was first described in Ref. [9]. If a condensate is placed in one of the two weakly-coupled spatially separated potential wells with matched energy levels, it can oscillate between the wells by linear quantum tunneling. However, due to atom-atom interactions, the tunneling is blocked when the number of atoms in the condensate exceeds some critical value. This suppression is due to the fact that interactions increase chemical potential of the atoms in the occupied wells and introduce nonlinear energy mismatch. Self trapping has been analyzed for a large number of systems including asymmetric double well potentials [10] and symmetric three well systems [11]. It has also been observed experimentally for atoms in a one dimensional optical lattice [12].

The quantum state of two trapped Bose-Einstein condensates in a double well potential has been analyzed in Ref. [13]. It has been shown that when the two wells are separated and the interaction between the atoms is repulsive, the lowest energy state is fragmented, which means that the coherence between the atoms in each well is lost. The dependence of this fragmentation on the splitting rate and physical parameters of the potential has been analyzed in Refs. [14] and [15]. The visibility of interference fringes after splitting of a condensate with both attractive and repulsive interactions was analyzed in Ref. [16], who showed a decrease in quantum noise in the case of attractive interactions. The quantum dynamics of atoms in a symmetric double well potential, where the atoms are in an initially fragmented state was also analyzed in [17].

Bose Einstein condensates in triple well structures have been analyzed and the stationary solutions in the mean field approximation were found in Ref. [18]. Three well systems show chaotic solutions [19] and the dynamics of atoms in a three well potential is sensitive to the initial conditions of the system [11]. This means that one can control the dynamics of the system not only by varying the physical parameters of the potential, but also by changing the initial conditions.

The authors of Ref. [20] have recently proposed a single atom transistor in a 1D optical lattice. A quantum interference phenomenon is used to switch the flux of atoms in a lattice through a cite containing a single impurity atom. Finally, Ref. [21] discusses "atomtronic" diodes and transistors which are direct analogs of their electronic counterparts. These devices use cold atoms in an optical lattice instead of electrons in a crystal. With the addition of impurities both N type and P type "semiconductors" may be constructed. A bipolar junction transistor could be then built with a NPN or PNP sandwich.

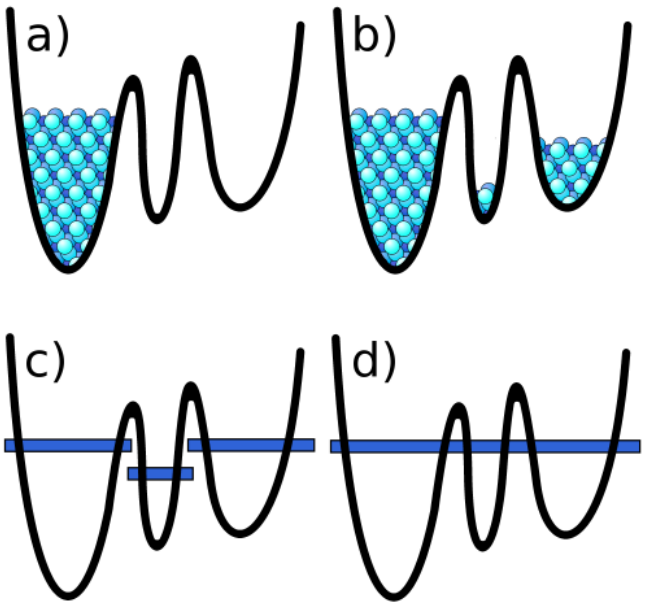

FIG. 1: The geometry of a BEC transistor. When the number of atoms in the middle well is small, tunneling from the left into the right well is negligible (a). This is due to the fact that the chemical potential of the middle well does not match that of the two other wells (c). Placing atoms in the middle well increases the chemical potential due to interatomic interactions (d) and enables tunneling then atoms tunnel from the left into the right well. This happpens because atom-atom interactions increase the energy of the middle guide (b).

The rest of the paper is organized as follows. Section II contains derivation of the general equations of motion for a BEC in an n-well potential with arbitrary shapes of the wells and discussion of the limits of validity of the model. In Sec. III we specialize our discussion to the case of a three well structure. Sec. III A is devoted to the analysis of the equations of motion in the mean field limit and in Sec. III B we will compare the results of the mean field to a second quantization calculation. Section IV contains estimates of the physical parameters for the device and discusses the possibility of its experimental realization.

II. EQUATIONS OF MOTION

The Hamiltonian for a system of interacting bosons in an external potential $V(x)$ is of the form

$$H = \int dx \hat{\Psi}^\dagger \left[-\frac{\hbar^2}{2m}\nabla^2 + V(x) \right] \hat{\Psi} + \frac{U_0}{2} \int dx \hat{\Psi}^\dagger \hat{\Psi}^\dagger \hat{\Psi} \hat{\Psi}. \quad (1)$$

Here $\hat{\Psi}$ is the field operator and $U_0 = 4\pi a_s \hbar^2/m$, where m is the atomic mass and a_s is the s-wave scattering

length. For notational simplicity we are considering one-dimensional case. Extension to two or three dimensions is straightforward.

In the standard basis of eigenfunctions ψ_i of the linear part of the Hamiltonian

$$\left[-\frac{\hbar^2}{2m}\nabla^2 + V(x)\right]\psi_i = \hbar\Omega_i\psi_i, \tag{2}$$

the field operator is represented as

$$\hat{\Psi} = \sum_i \psi_i a_i, \tag{3}$$

where a_i is the destruction operator for the mode ψ_i. These operators satisfy the canonical commutation relations

$$\begin{aligned}[a_i, a_j^\dagger] &= \delta_{ij},\\ [a_i, a_j] &= 0.\end{aligned} \tag{4}$$

The potential $V(x)$ consists of n weakly coupled potential wells. The eigenmodes ψ_i are "nonlocal" and extend over several potential wells. As discussed above, we are interested in calculating the number of atoms in each well as a function of time. A more convenient basis in this case corresponds to a set of modes ϕ_i localized in each potential well with the corresponding destruction operators b_i so that

$$\hat{\Psi} = \sum_i \phi_i b_i. \tag{5}$$

The operators b are linear superpositions of the operators a,

$$b_i = \sum_j u_{ji} a_j, \tag{6}$$

where u is the transformation matrix determined by the condition of localization of the modes ϕ_i.

Requiring that the destruction operators b_i satisfy the canonical commutation relations identical to those of Eq. (4)

$$\begin{aligned}[b_i, b_j^\dagger] &= \delta_{ij},\\ [b_i, b_j] &= 0,\end{aligned} \tag{7}$$

implies the unitarity of the transformation matrix u: $\sum_m u_{mi}u_{mj}^* = \delta_{ij}$. For bound states all modes ψ_i can be chosen real and the transformation matrix u can be chosen real and orthogonal.

The transformation from the "nonlocal" basis ψ_i to the "local" basis ϕ_i is given by the relations

$$\phi_i = \sum_j u_{ji}^* \psi_j. \tag{8}$$

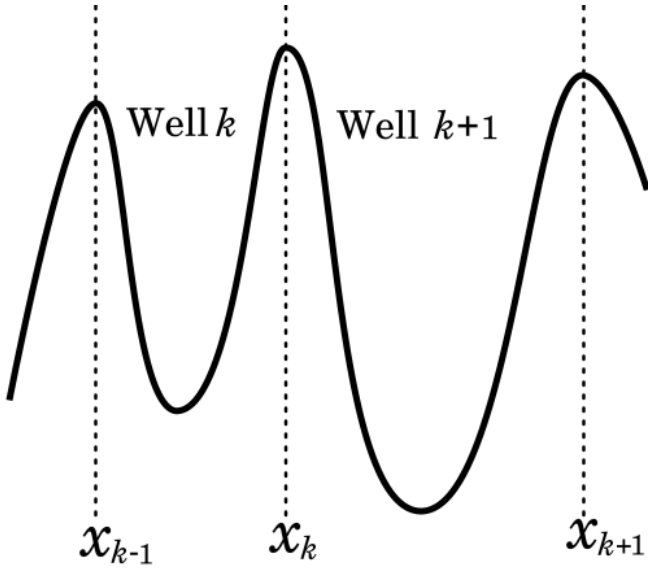

FIG. 2: A schematic of a multi-well non-symmetric potential structure with two adjacent wells shown. The points x_{k-1}, x_k and x_{k+1} are chosen between the wells where the eigenmodes ψ_k are exponentially small.

The operators b_i are associated with the local modes of the n-well structure. For the purposes of the subsequent analysis we will need to know only the lowest local mode in each potential well. It means that there are n local modes ϕ_i and the coefficients u_{ij} should be chosen so that the function ϕ_i be localized in the i-th potential well.

To quantify the degree of localization, we set points $x_0, x_1, ..., x_n$ somewhere between the wells where amplitudes of the modes ψ_k are exponentially small. This procedure is shown schematically in Fig. 2. The degree of localization of the mode ϕ_k in the k-th well is characterized by the localization parameter

$$f_k = \int_{x_{k-1}}^{x_k} dx|\phi_k|^2. \tag{9}$$

The localization parameter f_k can be rewritten in terms of the transformation matrix u as

$$f_k = \sum_{m,l} u_{mk}u_{lk}^* J_k(l,m), \tag{10}$$

where the matrix $J_k(l,m)$ is given by the expression

$$J_k(l,m) = \int_{x_{k-1}}^{x_k} dx\psi_m^*\psi_l. \tag{11}$$

To localize the modes ϕ_k, we maximize the function

$$f = \sum_k f_k = \sum_{kml} u_{mk}u_{lk}^* J_k(l,m) \tag{12}$$

subject to constraints

$$\sum_k u_{mk} u^*_{lk} = \delta_{ml}. \tag{13}$$

The maximization results in the set of n^2 equations

$$\sum_m \left[J_j(i,m) - \lambda_{im} \right] u_{mj} = 0, \tag{14}$$

where $1 \le i, j \le n$ and where $\lambda_{im} = \lambda^*_{mi}$ are Lagrangian multipliers.

The set of equations (14) can be written in a more transparent form as a set of n matrix equations ($j = 1, 2, \dots n$)

$$\left(\hat{J}_j - \hat{\lambda} \right) |u_j\rangle = 0, \tag{15}$$

where $\hat{J}_j$ and $\hat{\lambda}$ are Hermitian matrices with the elements $J_j(i,m)$ and λ_{im}, respectively, and where $|u_j\rangle$ is the column vector of u with the elements u_{mj} ($m = 1, 2, \dots n$). The equation of constraints, Eq. (13), becomes

$$\langle u_i | u_j \rangle = \delta_{ij}. \tag{16}$$

In the limit of negligibly small coupling between the wells, the column vectors $|u_k\rangle$ of the transformation matrix u are exact eigenvectors of the operators $\hat{J}_j$ because the latter in this limit reduce to $\hat{J}_j = |u_j\rangle\langle u_j|$. The matrix of Lagrange multipliers in this limit becomes the identity matrix. This observation suggests that for nonzero coupling between the wells the vectors $|u_k\rangle$ can be found perturbatively starting from the eigenvectors $|w_k\rangle$ of $\hat{J}_k$ with eigenvalues close to one:

$$\hat{J}_k |w_k\rangle = \mu_k |w_k\rangle = (1 - \epsilon a_k) |w_k\rangle, \tag{17}$$

where $\epsilon \ll 1$ characterizes relative coupling strength between the wells. The eigenvectors $|w_k\rangle$ form a nonorthogonal basis set with $\langle w_i | w_j \rangle = O(\epsilon)$ for $i \ne j$.

Solution of Eq. (17) in the $|u_k\rangle$ basis to the first order in ϵ yields

$$|w_k\rangle = |u_k\rangle + \sum_{j \ne k} |u_j\rangle \langle u_j | \hat{J}_k | u_k \rangle, \tag{18}$$

where we have used the fact that $\hat{J}_k - |u_k\rangle\langle u_k| = O(\epsilon)$. Inversion of Eq. (18) yields

$$|u_i\rangle = |w_i\rangle - \sum_{j \ne i} |w_j\rangle \langle u_j | \hat{J}_i | u_i \rangle, \tag{19}$$

Using the orthogonality conditions for $|u_i\rangle$ up to the first order in ϵ and the condition $\langle u_i | \hat{J}_j | u_j \rangle = \langle u_i | \hat{J}_i | u_j \rangle$ that follows from Eq. (15), results in the relation

$$\langle u_i | \hat{J}_j | u_j \rangle = \frac{1}{2} \langle w_i | w_j \rangle \tag{20}$$

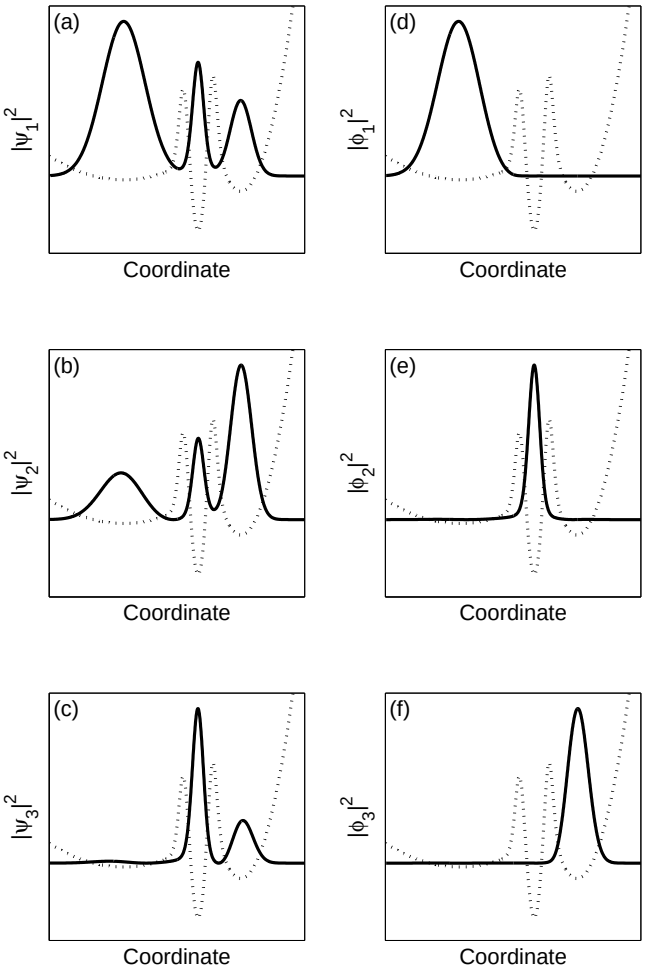

FIG. 3: An example of calculation of local modes. Graphs (a)-(c) show the three lowest global eigenmodes of the potential V (dotted line). These eigenmodes are nonlocal with large probability density in two or more wells. Graphs (d)-(f) show local modes, which are linear combinations of the nonlocal eigenmodes.

yielding the final expression for the vectors $|u_i\rangle$ in terms of $|w_i\rangle$:

$$|u_i\rangle = |w_i\rangle - \frac{1}{2} \sum_{j \ne i} |w_j\rangle \langle w_j | w_i \rangle. \tag{21}$$

To calculate the local modes, one thus finds eigenvectors $|w_i\rangle$ of $\hat{J}_i$ with eigenvalues close to one for $i = 1, 2, \cdots n$. The columns of the transformation matrix are then given by Eq. (21). The local modes are found using Eq. (8). An example of such calculation is shown in Fig. 3.

Overall signs of the local modes ϕ_i in Eq. (8) are arbitrary being determined by sign choices for the global modes ψ_i. These signs can be changed if needed because if ϕ_i is a local eigenmode, so is $-\phi_i$. Changing the sign of ϕ_i amounts to changing the sign of the i-th row of the transformation matrix u which leaves it unitary. To be able to unambiguously specify the value of the relative phase shift between condensates in different potential

wells, the overall signs of the local modes ϕ_i will be fixed by requiring that each eigenmode ϕ_i be positive in the region of its localization between x_i and x_{i+1}.

In terms of the destruction operators b_i of the local modes the Hamiltonian Eq. (1) can be written as

$$H = \sum_{ijk} \hbar\Omega_k u_{ki} u_{kj}^* b_i^\dagger b_j + \frac{U_0}{2} \sum_i \kappa_i \left(b_i^\dagger\right)^2 b_i^2, \qquad (22)$$

where Ω_i is the eigenfrequency of the i-th mode ψ_i given by Eq. (2), u_{ij} is the transformation matrix and κ_i is the overlap integral

$$\kappa_i = \int dx |\phi_i|^4. \qquad (23)$$

The equations of motion for the operators b_i in the Heisenberg picture are given by

$$i\hbar \frac{d}{dt} b_i = \sum_{jk} \hbar\Omega_k u_{ki} u_{kj}^* b_j + U_0 \kappa_i b_i^\dagger b_i^2. \qquad (24)$$

The diagonal terms

$$\Lambda_i = \sum_k \Omega_k |u_{ki}|^2 \qquad (25)$$

in Eq. (22) have the meaning of eigenfrequencies of the local eigenmodes in the absence of coupling between the wells and the nondiagonal terms

$$\Delta_{ij} = \sum_k \Omega_k u_{ki} u_{kj}^* \qquad (26)$$

are coupling frequencies between the i-th and j-th wells. Since for bound states u can be chosen real, the matrix of the coupling frequencies is real and symmetric: $\Delta_{ij} = \Delta_{ji}$. The coupling strength is exponentially dependent on the distance between the wells and usually only the nearest-neighbor coupling should be taken into account.

III. THREE-WELL STRUCTURE

In the following we shall specialize our analysis to the case of a potential consisting of three potential wells. These will be referred to as the left, middle and right well, respectively. The left well serves as a source of atoms. The number of atoms N_l in this well is kept nearly constant and is considerably larger than the number of atoms initially placed and subsequently tunneling into the middle or the right wells. The dynamics in the left well is therefore unaffected by that in the other two wells. This dynamics is factored out and the destruction operator for the left well b_l is replaced by a c-number: $b_l =\to \sqrt{N_l}$.

The Hamiltonian Eq. (22) reduces to

$$\begin{aligned} H &= \hbar(\Lambda_m - \mu) b_m^\dagger b_m + \hbar(\Lambda_r - \mu) b_r^\dagger b_r \\ &+ \hbar(\Delta_{lm}\sqrt{N_l} b_m + \Delta_{mr} b_m^\dagger b_r + h.c.) \\ &+ \frac{U_0}{2}\kappa_m \left(b_m^\dagger\right)^2 b_m^2 + \frac{U_0}{2}\kappa_r \left(b_r^\dagger\right)^2 b_r^2 \end{aligned} \qquad (27)$$

where Λ_i, Δ_i and κ_i are given by Eqs. (25), (26) and (23), respectively, *h.c.* means Hermitian conjugate and $\mu = \hbar\Lambda_l + \kappa_l U_0 N_l$.

As discussed at the end of Sec. II, the overall sign of the local modes ϕ_i has been fixed by requiring that they be positive in the region of their localization. With this choice, the coupling frequencies Δ_{ij} between different wells (see Eq. (26)) are negative. This is easily ascertained using the simplest example of a symmetric two-well structure where the two local modes are proportional to a sum and a difference of the two global modes. Normalizing the Hamiltonian Eq. (27) to the positive energy $-\hbar\Delta_{mr} = \hbar|\Delta_{mr}|$ brings it to its final dimensionless form

$$\begin{aligned} \frac{H}{\hbar|\Delta_{mr}|} &= \omega_m b_m^\dagger b_m + \omega_r b_r^\dagger b_r - (D b_m + b_m^\dagger b_r + h.c.) \\ &+ \frac{Z_m}{2}\left(b_m^\dagger\right)^2 b_m^2 + \frac{Z_r}{2}\left(b_r^\dagger\right)^2 b_r^2, \end{aligned} \qquad (28)$$

where $Z_i = -U_0\kappa_i/\hbar\Delta_{mr}$, $\omega_i = (\mu - \Lambda_i)/\Delta_{mr}$ and $D = \Delta_{lm}\sqrt{N_l}/\Delta_{mr}$.

The Heisenberg equations of motion for the destruction operators b_l and b_r (24) in the dimensionless variables take the form

$$\begin{aligned} i\frac{d}{d\tau} b_m &= (\omega_m + Z_m b_m^\dagger b_m) b_m - D - b_r \\ i\frac{d}{d\tau} b_r &= (\omega_r + Z_r b_r^\dagger b_r) b_r - b_m, \end{aligned} \qquad (29)$$

where the dimensionless time τ is given by the relation $\tau = |\Delta_{mr}|t$.

A. Mean-field

In this section we shall present results of analysis of Eq. (29) in the mean-field limit corresponding to relatively large atomic populations in all wells, when the operators b_m and b_r can be treated as complex numbers.

Figure 4 demonstrates control of atomic population in the right well by population in the middle well with the absolute gain that is considerably larger than one. Parameters for Fig. 4 are $\omega_m = -1.3$, $\omega_r = 0.5$, $Z_m D^2 = 1$ and $Z_r D^2 = 0$. The right well is initially empty, $b_r(0) = 0$. Parameters of the wells are chosen so that if no atoms are initially placed in the middle well ($b_m(0) = 0$), the tunneling from the source (the left well) to the middle well is strongly suppressed and the population in the right well remains at a low level. This situation is illustrated by a dotted line in Fig. 4.

Placing some number of atoms in the middle well results in a much larger tunneling rate from the left to the right well through the middle well as shown by a solid line corresponding to the initial condition $b_m(0) = D$. The increase in the tunneling rate can be observed for a range of values of the relative phase of the condensates in the left and middle wells. The dashed curve obtained

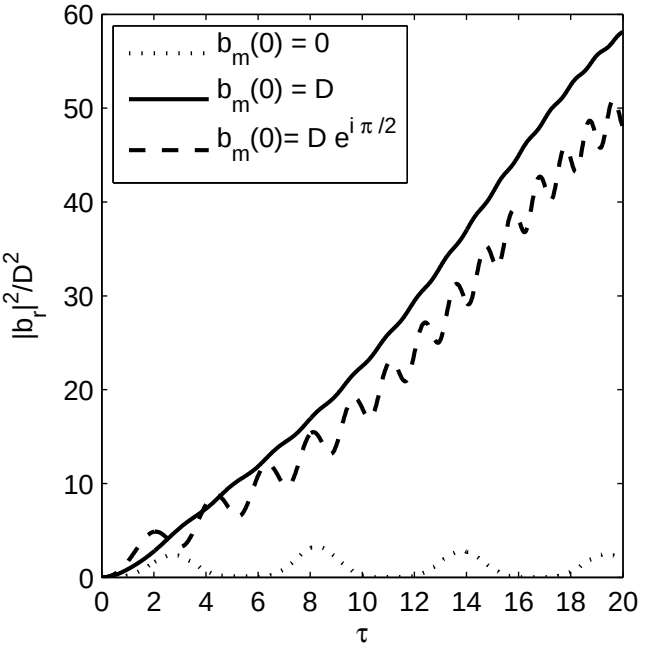

FIG. 4: The number of atoms in the right well as a function of interaction time for different initial number of atoms in the middle well. The dotted curve corresponds to initially empty middle well, $b_m(0) = 0$, and the solid curve to $b_m(0) = D$. The dashed curve corresponds to the initial condition $b_m(0) = D\exp(i\pi/2)$. For all curves $\omega_m = -1.3$, $\omega_r = 0.5$, $Z_m D^2 = 1$ and $Z_r D^2 = 0$.

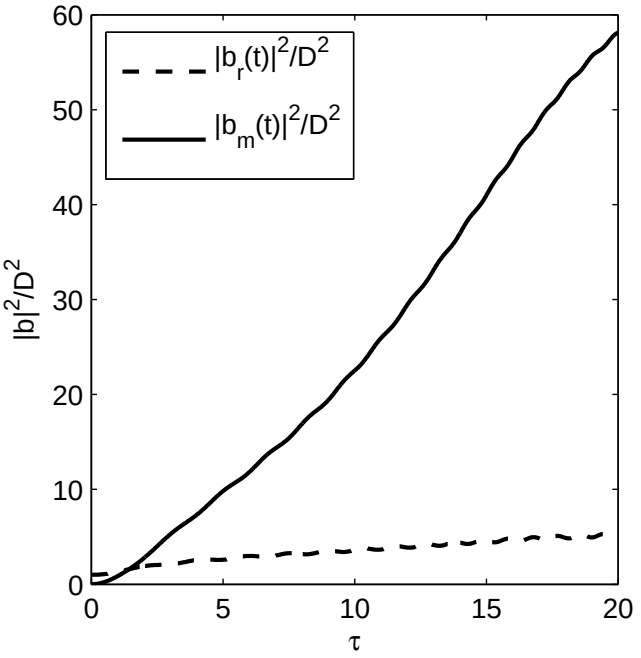

FIG. 5: The number of atoms in the middle (dashed) and right (solid curve) well as a function of interaction time for $\omega_m = -1.3$, $\omega_r = 0.5$, $Z_m D^2 = 1$, $Z_r D^2 = 0$ and $b_m = D$

for the initial condition $b_m(0) = D\exp(i\pi/2)$, i.e., corresponding to the $\pi/2$ relative phase shift between the condensates in the left and middle wells, exhibits qualitatively similar behavior. Note that the output number of atoms in the right well ($\tau = 20$) is about $50 - 60$ times larger than the input number of atoms in the middle well. In other words, the output number of atoms in the right is controlled by that in the middle well with the absolute gain $G = N_{r,out}/N_{l,in} \approx 50 - 60$.

Populations in the middle and right wells as functions of the interaction time are shown if Fig. 5 for $b_m(0) = D$. All other parameters are the same as in previous graphs. The solid curve is the population of the right well and the dashed curve is the population of the middle well. Figure 5 demonstrates that the population of the middle well stays about an order of magnitude below that for the right well. The middle well serves a gate controlling the rate of atomic flow from the source to the right well. The atoms tunneling from the source to the right well pass through the middle well without being accumulated there.

The output number of atoms in the right well as a function of the input number of atoms in the middle well is shown in Fig. 6. Parameters for this figure are the same as for Fig. 4, i.e., $\omega_m = -1.3$, $\omega_r = 0.5$, $Z_m D^2 = 1$ and $Z_r D^2 = 0$. The solid curve corresponds to the zero initial phase shift between the condensates in the left and middle wells and the dotted curve to the $\pi/2$ shift. This figure demonstrates rapid switching from small to large tunneling rates in the region around $|b_{m,in}|^2 D^2 \approx 0.5$ with subsequent saturation at the level $G = N_{r,out}/N_{m,in} \approx 50 - 60$. In the switching region, a small change in the population of the atoms in the middle well results in a large difference in the population in the right well.

Figure 7 shows output population in the right well ($\tau = 20$) as a function of the modal frequency ω_m of the middle guide for different values of the input number of atoms in the middle well. This figure demonstrates switching for different values of the number of atoms initially in the middle well. The dotted line corresponds to initially empty middle well. For this curve, the maximum tunneling rate corresponds to the region around $\omega_m = -0.5$. If the frequency of the middle well is lowered beyond this value, the number of atoms that tunnel into the right well becomes small. The solid curve corresponds to the initial condition $b_m(0) = D$. This curve is qualitatively similar to that for an initially empty middle well, but the maximum has moved to a lower value of $\omega_m = -1.3$. The dashed curve corresponds to the initial condition $b_m(0) = D\exp(i\pi/2)$. This curve still has a maximum around $\omega_m = -1.3$. For this value of ω_m, the number of atoms that tunnel into the right well when the initial atoms have either zero or $\pi/2$ phase shift is about the same. For the initially empty middle well, the population in the right well remains small.

As opposed to an electronic transistor, the amplifica-

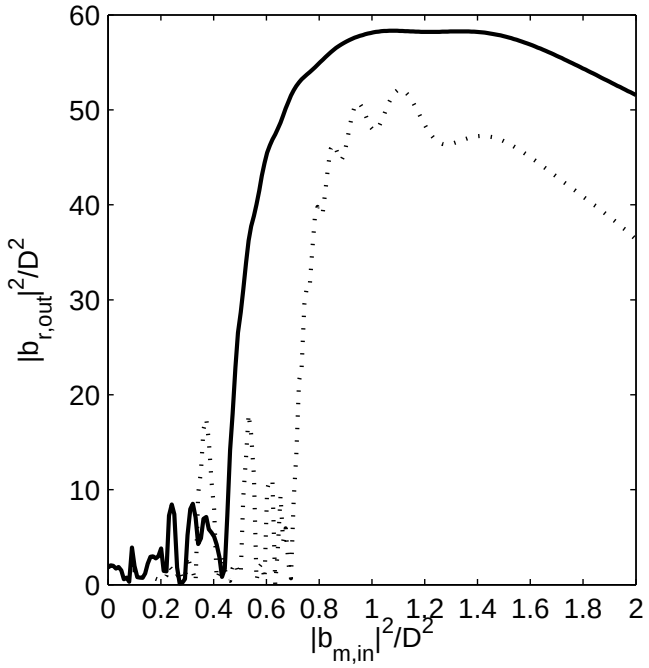

FIG. 6: The output number of atoms in the right well ($\tau = 20$) as a function of the number of atoms initially placed in the middle well.

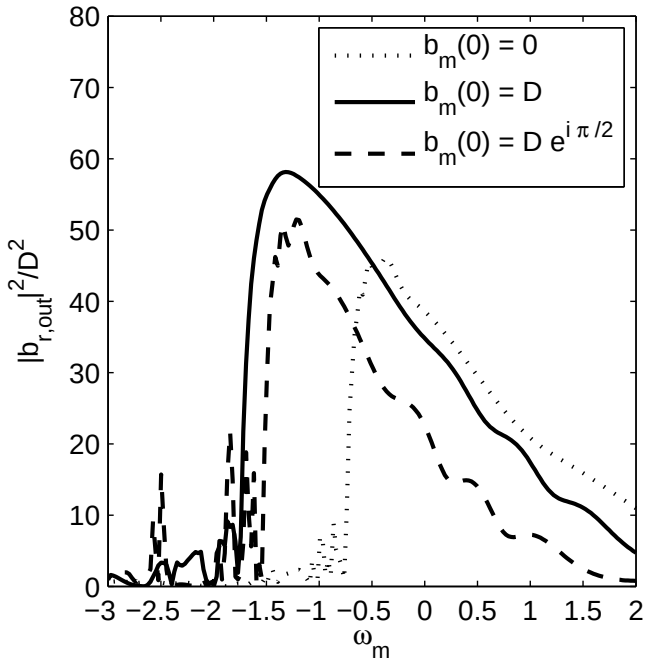

FIG. 7: The output number of atoms in the right well ($\tau = 20$) as a function of the frequency of the middle well ω_m. The dotted line corresponds to the initially empty middle well, $b_m(0) = 0$, the solid line to $b_m = D$, and the dashed line to $b_m = D\exp(i\pi/2)$.

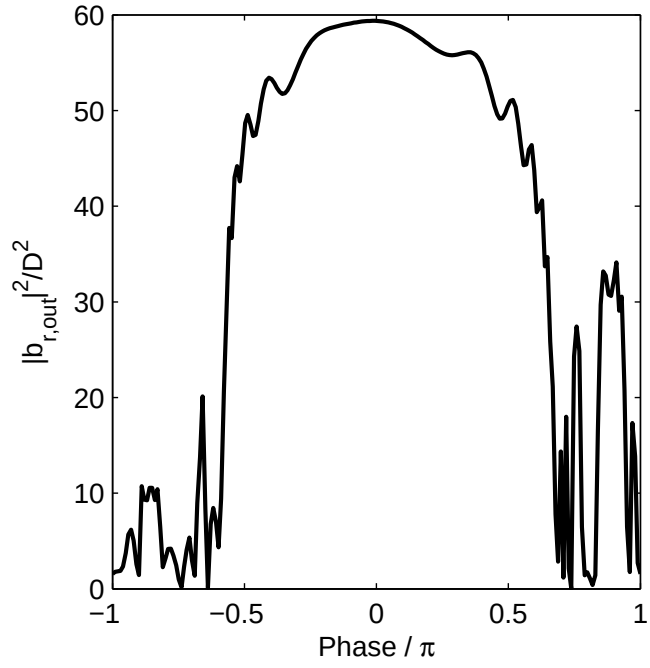

FIG. 8: The output number of atoms in the right well as a function of the relative phase of the atoms placed in the middle well.

tion and switching in the three-well structure is a coherent effect and depends on the relative phase between the condensates in the left and middle wells. To investigate sensitivity of the previously obtained results to the value of the relative phase angle, we kept the input number of atoms in the middle well fixed at $|A_m(0)/D|^2 = 1.2$ and changed the relative phase angle. The results are given by Fig. 8 showing the output number of atoms in the right well ($\tau = 20$) as a function of the phase angle. All other parameters are the same as in previous figures. Figure 8 demonstrates that in the amplification regime the number of atoms that tunnel into the right well is nearly independent of the initial phase angle, as long as this angle is roughly in the range between $-\pi/2$ and $\pi/2$.

B. Second-quantization results

This section presents results of analysis of the three-well structure in the framework of the second-quantization formalism. This allows us to estimate the region of applicability of the mean-field approach of section III A, evaluate intrinsic quantum-mechanical uncertainty due to finite number of atoms and extend previous results to the limit of small number of atoms.

In the dimensionless variables, the state vector of the system $|\psi(t)\rangle$ evolves according to the equation

$$i\frac{d}{d\tau}|\psi\rangle = H|\psi\rangle, \tag{30}$$

where H is the second-quantized Hamiltonian given by

Eq. (28). The state vector can be represented in terms of the joint number states $|n_m, n_r\rangle$ as

$$|\psi\rangle = \sum_{i,j} c_{i,j}|n_i, n_j\rangle, \tag{31}$$

with the decomposition coefficients given by $c_{m,r} = \langle n_m, n_r|\psi\rangle$. Equation (30) is transformed to the set of ordinary differential equations that describe the evolution of the decomposition coefficients

$$i\frac{d}{d\tau}c_{i,j} = \sum_{i,j,k,l} \langle n_i, n_j|H|n_k, n_l\rangle c_{k,l}. \tag{32}$$

In simulations, the set of Eqs. (32) has been truncated by keeping only the values of n_m and n_r such that $n_r + n_m \leq N_{max}$. The value of N_{max} was chosen so that N_{max} was several times larger than the sum $\langle n_r\rangle + \langle n_m\rangle$.

Initial conditions for the system of equations Eq. (32) corresponded to zero initial number of atoms in the right well with the atoms in the middle well being in a coherent state:

$$|\psi(0)\rangle = e^{-|\alpha|^2} \sum_{n=0}^{N_{max}} \frac{\alpha^n}{\sqrt{n!}}|n, 0\rangle. \tag{33}$$

Here the complex parameter α is given by $\alpha = \sqrt{\langle N_m\rangle(0)}e^{i\varphi}$, where $\langle N_m\rangle(0)$ is the average number of atoms initially placed in the middle well and φ is the phase difference between the atoms in the middle and left wells.

The transition to the mean-field limit corresponds to increasing the input number of atoms in the middle well $\langle N_m\rangle(0)$ while keeping the ratio $\omega_m/Z_m\langle N_m\rangle(0)$ constant. Equations (28) show that the results of action of the destruction operators on the state vector scales as D provided the parameters $Z_m D^2$ and $Z_r D^2$ are kept constant. Thus, the transition to the mean-field limit can be implemented by setting the initial number of atoms in the middle well proportional to D^2 and increasing the value of coupling D between the left and middle wells while keeping the parameters $Z_m D^2$ and $Z_r D^2$ constant.

The average number of atoms in the right well $\langle N_r\rangle$ as a function of the interaction time is shown in Fig. 9 for three different values of D^2. The parameters for this figure are $\omega_r = 1$, $\omega_m = -0.5$, $Z_m D^2 = 1/4$, $Z_r D^2 = 0$ and $|\alpha|^2 = \langle N_m\rangle(0) = D^2$. The phase angle of the coherent state is zero. The solid line is the mean-field limit. The dotted, dash-dotted and dashed lines correspond to $D^2 = 1$, $D^2 = 4$ and $D^2 = 8$, respectively. Figure 9 demonstrates good convergence of the second-quantization results to the mean field limit as D^2 is increased. The $D^2 = 1$ curve deviates from the mean-field limit for large value of τ, but all other curves lie progressively closer to the mean-field curve as the parameter D increases.

The output ($\tau = 10$) probability distribution $P(N_r)$ of finding N_r atoms in the right well versus N_r is shown if

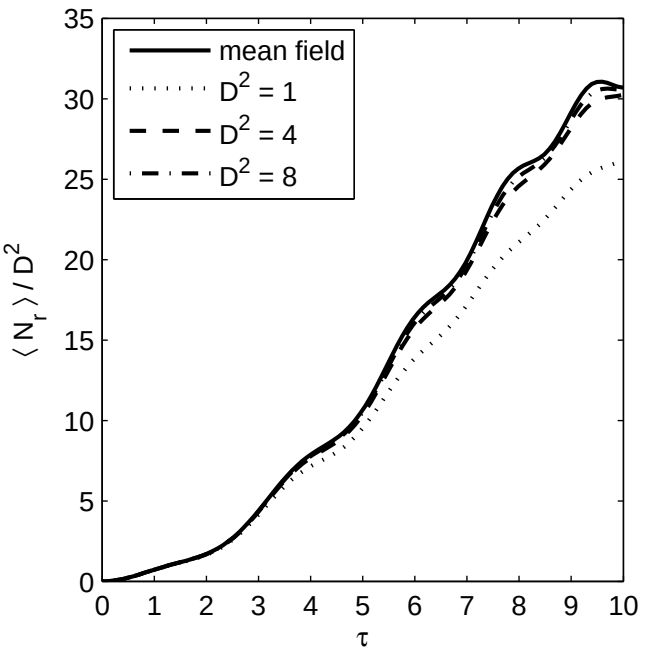

FIG. 9: The average number of atoms in the right well as a function of the interaction time for three different values of the coupling between the left and the middle wells. Atoms in the middle well are initially in a coherent state with $\langle N_m\rangle(0) = D^2$ and zero phase. The solid line is the result of the mean-field calculation, the dotted line is the result of the second-quantization calculation with $D^2 = 1$, the dashed line corresponds to $D^2 = 4$, and the dash-dotted one to $D^2 = 8$.

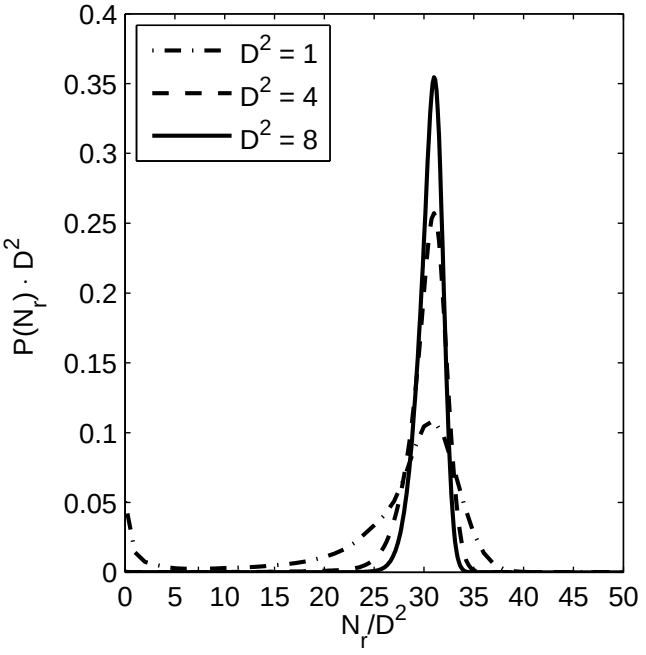

FIG. 10: The probability $P(N_r)$ of finding N_r atoms in the right well ($\tau = 10$). Atoms in the middle well are initially in a coherent state with $\alpha = D$. The dash-dotted line corresponds to $D^2 = 1$, the dashed line to $D^2 = 4$ and the solid line to $D^2 = 8$.

Fig. 10. The dash-dotted line corresponds to $D^2 = 1$, the dashed line to $D^2 = 4$ and the sold line to $D^2 = 8$. Since the number of output atoms scales as D^2, the horizontal axes is scaled as N_r/D^2 to keep position of the maximum and the width of the curves more of less the same for different values of D^2. As a result, the vertical axes shows not $P(N_r)$, but the product $P(N_r)D^2$ to keep the height of the curves approximately the same for different values of D^2. The total "area under the curve" (strictly speaking it is a sum, not an integral) for all curves is equal to one. The dash-dotted curve corresponding to $D^2 = 1$ shows bimodal distribution with a relatively large probability of finding atoms near zero N_r in addition to the main peak near $N_r/D^2 \approx 31$, the latter being very close to the mean-field result. The difference between the mean-field and second-quantization results, previously seen in Fig. 9 for $D^2 = 1$, is due to the part of the probability distribution near zero that pulls down the average. As the coupling D to the source is increased, only the single-humped part of the probability $P(N_r)$ centered at the mean-field result remains. The output relative standard deviation $\Delta N_r/\langle N_r\rangle$ is equal to 0.35, 0.08 and 0.04 for $D^2 = 1, 4$ and 8, respectively.

Comparison of the mean-field and second-quantization results carried out for the same parameters as above but the relative phase angle between the condensates equal to $\phi = \pi/2$ yielded conclusions very similar to those summarized by Figs. 9 and 10.

Figures 11 and 12 parallel analysis of Figs. 9 and 10 for the case when the middle well is initially empty, $|\alpha|^2 = \langle N_m\rangle(0) = 0$. These figures are aimed at verifying that the rapid switching from low to high-amplification regime predicted by the theory in the mean-field limit can be also realized with only few controlling atoms.

Figure 11 demonstrates convergence of the second-quantization results to the mean-field limit for $\langle N_m\rangle(0) = 0$ as D^2 is increased. This convergence is similar to that shown in Fig. 9 except in this case the second-quantization approach gives values somewhat larger than the mean-field limit. The reason is explained by Fig. 12, which shows the probability $P(N_r)$ of finding N_r atoms in the right well at $\tau = 10$. The probability $P(N_r)$ has a pronounced spike at low values of N_r. Another noticeable feature of Fig. 12 is a wide, nearly flat pedestal extending from small values of N_r to a maximum value that is about twice larger than the average (cf. Fig. 11). The maximum value slightly decreases as D increases. This explains why the second-quantization results are larger than the mean-field results. The one-humped shape of $P(N_r)$ in Fig. 10 means that the uncertainty in the output number of atoms in the high-amplification regime is small for even a few controlling atoms in the middle well. Figures 11 and 12 show that the low-amplification region is characterized by both low average number of output atoms and by large uncertainty corresponding to the average. Indeed, the output relative standard deviation $\Delta N_r/\langle N_r\rangle$ for the results of Fig. 12 is equal to 1.3, 1.0 and 0.9 for $D^2 = 1, 4$ and 8, respectively. These re-

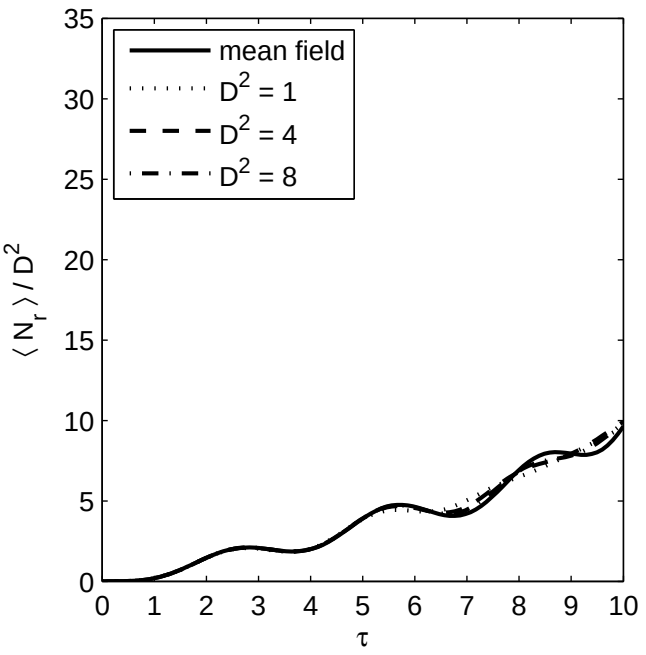

FIG. 11: The average number of atoms in the right well as a function of the interaction time for three different values of the coupling between the left and the middle wells. The middle well is initially empty. The solid curve is the result of the mean-field calculation, the dotted curve is the result of the second-quantization calculation with $D^2 = 1$, the dashed curve corresponds to $D^2 = 4$, and the dash-dotted curve to $D^2 = 8$.

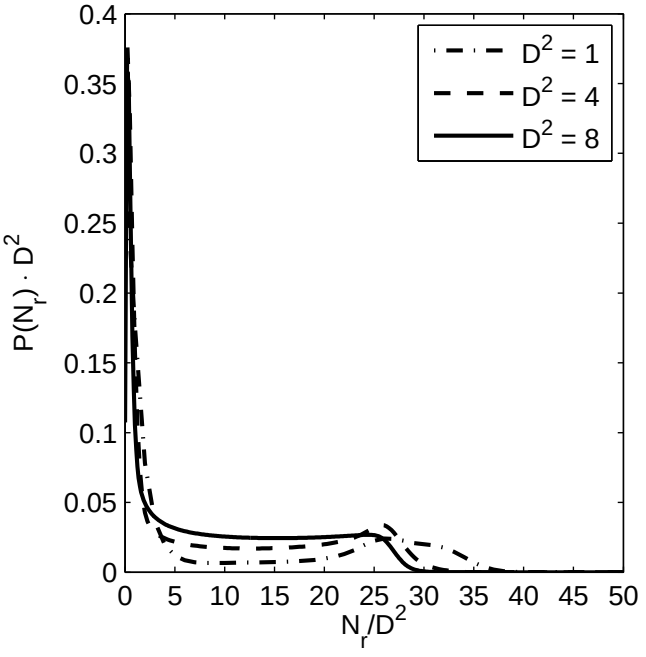

FIG. 12: The probability $P(N_r)$ of finding N_r atoms in the right well ($\tau = 10$). The middle well is initially empty. The dash-dotted line corresponds to $D^2 = 1$, the dashed line to $D^2 = 4$ and the solid line to $D^2 = 8$.

sults are in contrast to those for the large-amplification regime of Fig. 10, where the standard deviation rapidly goes down as the parameter D^2 increases.

IV. DISCUSSION

The analysis of Sec. III demonstrates that a Bose Einstein condensate in a three well potential shows transistor-like behavior with the middle well acting as a gate controlling the flux of atoms from the source to the drain. In this section we present estimates of the characteristic tunneling time for a trapped atom transistor and discuss possible gain in the total number of atoms. The analysis will be extended to the case of a waveguide device, where estimates will be presented for the tunneling time, the length of the device and the gain in the output flux of atoms. Finally, we summarize the results obtained.

A. Trapped atom transistor

The parameter D in Eq. (29) characterizes the strength of coupling of the source (left well) to the gate (medium well). It is reasonable to expect that the operational parameters of the BEC transistor are such that the contributions of the nonlinear and linear terms in Eq. (29) are of the same order of magnitude, i.e. $Z_m D^2 \approx 1$.

The growth curve, shown if Fig. 6 shows the final population of the right well as a function of the initial population of the middle well, where the atoms are held in the traps for a dimensionless time $\tau = 20$. This figure demonstrates that a change in the population of the middle well from $N_m = 0.4D^2$ to $N_m = 0.8D^2$ results in a change in the final population of the right well from $N_r \approx 10D^2$ to $N_r \approx 60D^2$. The maximum number of atoms that tunnel into the right occurs when the number of atoms initially in the middle well is $N_m \approx D^2$. We will refer to this number as the saturation number. For example, if we take $D^2 = 10$, a change from 4 to 8 atoms in the middle well results in a change from 100 to 600 atoms in the right well.

Assume that the potential energy of the middle well is a cigar shaped potential of the form

$$V(r_\perp, z) = \frac{1}{2} m \left(\omega_\perp^2 r_\perp^2 + \omega_z^2 z^2\right), \tag{34}$$

where $r_\perp$ is the coordinate in the radial direction, and z is the coordinate in the axial direction. For this potential, the overlap integral given by the Eq. (23) can be evaluated as

$$\kappa_m = \frac{1}{(2\pi)^{3/2}} \frac{1}{a_\perp^2 a_z}, \tag{35}$$

where $a_\perp = \sqrt{\hbar/m\omega_\perp}$ and $a_z = \sqrt{\hbar/m\omega_z}$ are the harmonic oscillator lengths. The nonlinearity parameter Z_m in Eq. (28) is given by the expression

$$Z_m = \frac{U_0 \kappa_m}{\hbar |\Delta_{mr}|}, , \tag{36}$$

where $U_0 = 4\pi a_s \hbar^2/m$. Using Eq. (35) in Eq. (36) allows one to express the tunneling frequency between the middle and the right wells as

$$|\Delta_{mr}| = a_s \frac{N_m}{a_z} \omega_\perp, \tag{37}$$

where we have also used $Z_m N_m \approx 1$ to eliminate Z_m in favor of N_m.

If the middle well is a spherical trap with $\omega_z = \omega_\perp = 2\pi \times 10^3 Hz$ and the saturation number is $D^2 = 10$ the tunneling frequency between the middle and right well is

$$\Delta_{mr} \approx \pi \times 10^2 rad/sec. \tag{38}$$

The dimensional time that it takes for atoms to tunnel from the left to the right wells is

$$t \approx 2 \times 10^{-1} sec. \tag{39}$$

In other words, for the parameters chosen a trapped atom transistor can distinguish between 4 and 8 atoms in the gate with the characteristic operational time of $10^{-1} sec$. This time can be decreased either by increasing the frequency of the trap or increasing the value of the saturation number.

B. Waveguide transistor

In a waveguide transistor the potential wells of Fig. 1 are the three guides that run parallel to each other for the distance L. The interaction time $T = L/v$ is determined by the speed of flow v of the BEC in the guides. The field operator for this configuration can be expressed as

$$\hat{\Psi}(\mathbf{r}, t) = \exp(i k_p z - i\omega_p t)\hat{\psi}(\mathbf{r}, t), \tag{40}$$

where k_p and $\omega_p = \hbar k_p^2/2m$ and the carrier wave number and frequency, respectively, and $\hat{\psi}$ is the field-operator envelope.

The Heisenberg equations of motion for the field operator $\hat{\psi}$ in the co-propagating frame $t' = t$, $z' = z - vt$ is of the form

$$i\hbar \frac{\partial}{\partial t}\hat{\psi} = \left[-\frac{\hbar^2}{2m}\left(\nabla_\perp^2 + \frac{\partial^2}{\partial z^2}\right) + V(\mathbf{r}_\perp) + U_0 \hat{\psi}^\dagger \hat{\psi}\right]\hat{\psi}, \tag{41}$$

where $v = \hbar k_p/m$ is the velocity of the condensate and the primes have been omitted.

Changes in density as the condensate propagates through the transistor occur at a length scale L_{BEC}. We assume that the kinetic energy associated with the longitudinal direction is small in comparison with the

characteristic energy $\hbar\Omega$ associated with the transverse eigenmodes of the transistor

$$\hbar\Omega \gg \frac{\hbar^2}{2mL_{BEC}^2}. \tag{42}$$

Next, we require that L_{BEC} does not change appreciably during the time interval L/v that it takes the condensate to propagate through the transistor,

$$\left|\frac{\partial}{\partial t}\ln L_{BEC}\right| \ll \frac{v}{L} \tag{43}$$

With Eqs. (42) and (43) fulfilled, the dispersive term $(\partial^2/\partial z^2)$ in Eq. (41) can be neglected and the coordinate z becomes a parameter. Propagation of different "slices" of the condensate (parametrized by the coordinate z) through the transistor can be analyzed independently.

Represent the field operator $\hat{\psi}$ as

$$\hat{\psi} = \sum_i \phi_i(\mathbf{r}_\perp) b_i(z,t), \tag{44}$$

where $\phi(\mathbf{r}_\perp)$ is the i-th transverse local mode and $b_i(z,t)$ is the destruction operator that destroys an atom in the i-th local mode at the coordinate z. Note that b_i now has dimension of $m^{-1/2}$.

Using Eq. (44) in Eq. (41) with the dispersive term dropped, results in the equations of motion in the Heisenberg picture for the operators b_i that are of the same form as Eq. (24):

$$i\hbar\frac{d}{dt}b_i(z,t) = \sum_{i,j}\hbar\Omega_k u_{ki}u_{kj}^* b_j + U_0\kappa_i b_i^\dagger b_i, \tag{45}$$

As in the case of a trapped device, the left guide will be treated as a reservoir of atoms corresponding to the replacement $b_l \to \sqrt{n_l}$, where n_l is the density of atoms (number of atoms per unit length). The equations of motion for the atoms in the middle and right guide, in dimensionless form, become

$$\begin{aligned} i\frac{d}{d\tau}b_m(z,t) &= (\omega_m + Z_m b_m^\dagger b_m)b_m - D - b_r \\ i\frac{d}{d\tau}b_r(z,t) &= (\omega_r + Z_r b_r^\dagger b_r)b_r - b_m, \end{aligned} \tag{46}$$

where the dimensionless parameters are $Z_i = -U_0\kappa_i/\hbar L\Delta_{mr}$, $\omega_i = (\mu - \Lambda_i)/\Delta_{mr}$, $D = \Delta_{lm}\sqrt{Ln_l}/\Delta_{mr}$, and L is the length of the transistor. The destruction operators are normalized to $b_i' = b_i/\sqrt{L}$, and the primes have been dropped. Since the equations for each "slice" in z are of the same form as Eq. (29), the analysis of Sec. III is valid for each "slice" separately.

As with the case of a trapped atom transistor, we take $Z_m D^2 = 1$ and use the fact that the largest tunneling rate corresponds to $n_m \approx D^2$. We refer to this as the saturation density, since n_m is the normalized density of atoms and not the total number as it was with a trapped atom device. Next, we assume that the middle waveguide can be described by the potential

$$V(\mathbf{r}_\perp) = \frac{1}{2}m\omega_\perp^2 r_\perp^2, \tag{47}$$

where $\omega_\perp$ is the transverse frequency of the guide. The overlap integral associated with this potential is

$$\kappa_m = \frac{1}{2\pi}\frac{1}{a_\perp^2}, \tag{48}$$

where $a_\perp$ is the transverse oscillator length and $a_\perp = \sqrt{\hbar/m\omega_\perp}$. Using Eq. (36) and (48), we evaluate the coupling frequency between the middle and right guides as

$$|\Delta_{mr}| \approx a_s\omega_\perp\frac{n_m}{L}. \tag{49}$$

In terms of the velocity of the atoms v and the flux entering the middle guide Φ_m the density can be expressed as $n_m/L = \Phi_m/v$, and Eq. (49) takes the form

$$|\Delta_{mr}| \approx a_s\omega_\perp\frac{\Phi_m}{v}. \tag{50}$$

Assuming that the guide has a transverse frequency of 10 kHz, the velocity 5 cm/sec and the saturation flux is 10^5 atoms/sec, we can evaluate the coupling frequency between the right and middle guide as

$$\Delta_{mr} \approx 2\pi \times 10^2 rad/sec. \tag{51}$$

The dimensional switching time is

$$t \approx 2 \times 10^{-1} sec, \tag{52}$$

and the length of the device is

$$L \approx 1cm. \tag{53}$$

This length can be decreased by slowing the velocity of the atoms, increasing the saturation flux or increasing the transverse frequency of the waveguide.

With the above numbers, a change in the input flux of the middle guide from 0.4×10^5 atoms/sec to 0.8×10^5 atoms/sec results in a change of flux in the output of the right guide from 10^6 atoms/sec to about 10^7 atoms/sec.

To summarize, we have presented a theoretical analysis of a Bose Einstein condensate in a nonsymmetric three-well potential which shows transistor-like behavior. We demonstrated the control of atomic population in the right well by the population in the middle well with an absolute and differential gains considerably larger than one. The second-quantization formalism was then used to evaluate the quantum-mechanical uncertainty due to a finite number of atoms and extend the mean-field results to the limit of a small number of atoms.

The BEC transistor can turn out to be useful in precision measurements. The number of atoms that tunnel

from the source to the drain is very sensitive to the number of atoms in the gate. This fact can be used to detect and amplify small changes in the number of atoms in the gate. A waveguide based transistor is capable of operating continuously and can be used to measure time-dependent phenomena. Applications of this device may include measurement of inertial changes and electromagnetic fields. It is possible to envision potentially more interesting applications by combining several such devices so that, e.g., the amplified output of the first transistor serves as control for the second.

V. ACKNOWLEDGEMENTS

This work was supported by the Defense Advanced Research Projects Agency's Defense Science Office through a PINS program (Grant No. W911NF-04-1-0043) and the Air Force Office of Scientific Research (Grant No. FA9550-04-1-0460).

[1] D. Müller, D. Z. Anderson, R. J. Grow, P. D. Schwindt, and E. A. Cornell, Phys. Rev. Lett. **83**, 5194 (1999).
[2] N. H. Dekker, C. S. Lee, V. Lorent, J. H. Thywissen, S. P. Smith, M. Drndic, R. M. Westervelt, and M. Prentiss, Phys. Rev. Lett. **84**, 1124 (2000).
[3] D. Cassettari, B. Hessmo, R. Folman, T. Maier, , and J. Schmiedmayer, Phys. Rev. Lett. **85**, 5483 (2000).
[4] A. E. Leanhardt, A. P. Chikkatur, D. Kielpinski, Y. Shin, T. L. Gustavson, W. Ketterle, and D. E. Pritchard, Phys. Rev. Lett. **89**, 040401 (2002).
[5] W. Hänsel, P. Hommelhoff, T. Hansch, and J. Reichel, Nature **413**, 498 (2001).
[6] W. Hansel, P. H. W. Hänsel, T. Steinmetz, T. Hansch, and J. Reichel, New Journal of Physics **7**, 3 (2005).
[7] Y.-J. Wang, D. Z. Anderson, V. M. Bright, E. A. Cornell, Q. Diot, T. Kishimoto, M. Prentiss, R. A. Saravanan, S. R. Segal, and S. Wu, Phys. Rev. Lett. **94**, 090405 (2005).
[8] Y. Shin, M. Saba, T. A. Pasquini, W. Ketterle, D. E. Pritchard, and A. E. Leanhardt, Phys. Rev. Lett. **92**, 050405 (2004).
[9] G. J. Milburn, J. Corney, E. M. Wright, and D. F. Walls, Phys. Rev. A **55**, 4318 (1997).
[10] A. Smerzi, S. Fantoni, S. Giovanazzi, and S. R. Shenoy, Phys. Rev. Lett. **79**, 4950 (1997).
[11] R. Franzosi and V. Penna, Phys. Rev. A **65**, 013601 (2001).
[12] T. Anker, M. Albiez, R. Gati, S. Hunsmann, B. Eiermann, A. Trombettoni, and M. K. Oberthaler, Phys. Rev. Lett. **94**, 020403 (2005).
[13] M. J. Steel and M. J. Collett, Phys. Rev. A **57**, 2920 (1998).
[14] R. W. Spekkens and J. E. Sipe, Phys. Rev. A **59**, 3868 (1999).
[15] J. Javanainen and M. Y. Ivanov, Phys. Rev. A **60**, 2351 (1999).
[16] M. Jaaskelainen, W. Zhang, and P. Meystre, Phys. Rev. A **70**, 063612 (2004).
[17] M. Jaaskelainen and P. Meystre, Phys. Rev. A **71**, 043603 (2005).
[18] K. Nemoto, C. Holmes, G. J. Milburn, and W. J. Munro, Phys. Rev. A **63**, 013604 (2000).
[19] R. Franzosi and V. Penna, Phys. Rev. E **67**, 046227 (2003).
[20] A. Micheli, A. J. Daley, D. Jaksch, and P. Zoller, Phys. Rev. Lett. **93**, 140408 (2004).
[21] B. T. Seaman, M. Kraemer, D. Z. Anderson, and M. J. Holland (2006), cond-mat/0606625.